

RESEARCH

Open Access



Triaxial testing and hydraulic–mechanical modeling of sandstone reservoir rock in the Upper Rhine Graben

Robert Egert* , Robin Seithel, Thomas Kohl and Ingrid Stober

*Correspondence:
robert.egert@kit.edu
Institute of Applied
Geosciences, Karlsruhe
Institute of Technology,
Adenauerring 20b,
76131 Karlsruhe, Germany

Abstract

The Upper Rhine Graben (URG) is a highly favorable location for deep geothermal energy utilization. One of the main reservoir horizons is the lower Triassic Buntsandstein formation. While quantification of thermal and hydraulic parameters and their coupling is common, geomechanical factors are often neglected due to high costs and the expense in gathering data. Equivalent experiments with analog rocks, like triaxial tests, can help to improve this knowledge. Triaxial tests have been performed and evaluated on two different Buntsandstein rock examples as analogs to quantify the mechanical behavior under stress conditions found in the Buntsandstein of the URG. Both samples, Tennenbach (TenSst) and Pfinztal (PfSst) Sandstone, show high Young's moduli under axial loading. With confining pressures up to 90 MPa, the axial failure strength is up to 448 (TenSst) and 561 (PfSst) MPa. The results demonstrate the usability of linear elasticity for the expected stress range in the Buntsandstein reservoir of the URG. The deformation behavior is described and a linear failure criterion is derived, predicting failure strength with a high accuracy. These experimental results can be further employed as calibration parameters for a hydro-mechanical evaluation of the deformation processes.

Keywords: Triaxial test, HM modeling, Mechanical characterization, Hydraulic implication, Buntsandstein, Upper Rhine Graben, Geothermal energy

Background

The determination of the subsurface conditions and reservoir properties is indispensable for exploration and exploitation of a geothermal field. It includes the expected geological structures as well as the hydraulic, thermal, chemical and mechanical parameters of the target horizon which should be favorable for geothermal utilization. Most essential is a high permeability to supply sufficient flow rates and high temperatures (Stober and Bucher 2012). An area in Germany which fulfills the criteria is the Upper Rhine Graben with a unique geothermal potential (Agemar et al. 2014). Local temperature anomalies with elevated temperatures up to 165 °C are expected at a depth of 2500 m, while the average geothermal gradient of the URG is above 40K km⁻¹ (Agemar et al. 2013). Especially the sedimentary formation of the Triassic, Buntsandstein and Muschelkalk shows high permeabilities, which are necessary to provide high flow rates (Stober and Bucher 2014).

However, the estimation of the geothermal potential of a reservoir from averaged data leads to high engineering risks. Mostly, pointwise distributed data are collected from few exploration wells and interpolated in the surrounding area, while horizontal and vertical heterogeneities are unknown (Fitch et al. 2015). Interpretation of geophysical data, like 2D or 3D seismic measurements, can provide spatial information, but is limited to larger structures, like faults or horizons, while fractures and small-scale heterogeneities are unresolvable (Mansfield and Cartwright 1996). Preliminary studies on analog rocks can help to decrease this risk by filling the gap between point data and reservoir scale (Philipp et al. 2008). Triaxial tests offers the opportunity to estimate the rock strength of a potential rock masses to reduce risks for wellbore and reservoir stability (Lama and Vutukuri 1978).

While these analog tests offer unique data averaged for the whole sample, sophisticated numerical methods are required for reservoir scale evaluations. Simulations are used to analyze mechanical and hydraulic processes and their linkage between each other in detail and to quantify their influence on both the results and vice versa (Rutqvist et al. 2002). The recent progress in hardware and software development allows calculating the complex coupling of physical processes in a natural and perturbed geoscientific environment at efficient computation times (Kohl and Hopkirk 1995; O'Sullivan et al. 2001; Watanabe et al. 2017). The experimental results of different tests, like triaxial or permeability tests, carried out with a permeameter can also be used as input and calibration parameters to upscale the laboratory to reservoir data (Settari et al. 2013).

The goal of our investigation is the identification of the geomechanical and hydraulic parameters of the geothermal Buntsandstein reservoir in the URG to better characterize the processes which take place during deformation and stress field changes inside the rocks. Numerical investigations, based on the mechanical properties of two comparative rock samples, Tennenbach und Pfinztal Sandstone, have been performed to investigate their mechanical behavior and to quantify the influence on hydraulic properties, namely permeability and porosity, in a scale-independent manner. The advantage of the coupled numerical investigation is the possibility to use and combine independent experimental setups and data, while combined measurements of deformation and permeability are lengthy and expensive. Different uncertainties, regarding the linking between sample-scale failure prediction and the reservoir-related stress regime and the hydro-mechanical connection between mechanical and hydraulic parameters, are thoroughly investigated to fill the gap between the sample-scale and reservoir engineering issues.

Geological overview

Upper Rhine Graben

The Upper Rhine Graben (URG), as a main geothermal target, is an NNE-SSW to N-S-striking graben structure in the central part of the 1100 km extended European Cenozoic rift system (Illies 1965; Pflug 1982). The evolution of the URG is related to polyphase reactivations of lithospheric crustal discontinuities since the late Paleozoic (Ziegler and Dèzes 2005). The main phase of tectonic rifting starts in the middle Eocene with an NW-SE extension of the upper crust and the reactivation of the Permo-Carboniferous and variscan discontinuities, which lead to SW-NE striking stress regime (Ziegler et al. 2004). In the Miocene, the regional stress field changes to an NW-SE sinistral

transtensional regime with reactivation of the older fault system (Illies 1972). Starting from the northern part, the URG was subjected to large subsidence and sedimentation up to 3.5 km (Grimmer et al. 2017).

There are two reservoir lithologies for the utilization of geothermal energy in the URG. The crystalline basement, e.g., granite, can be utilized as an enhanced geothermal reservoir, like in Soultz-sous-Forêts (Held et al. 2014), and the higher porous and conductive sedimentary formations, like Buntsandstein or Muschelkalk, as hydrothermal reservoir, like Bruchsal (Meixner et al. 2014). High flow rates, especially in fracture or fault systems, are expected in the URG to achieve geothermal usage.

The recent stress field in the URG is characterized by an NW–SE orientation with local variations. The northern part of the URG with an orientation from N130°E to N135°E is characterized by normal faulting, while in the southern part, striking N145°E–N160°E, a transition from strike-slip to normal faulting is observed (Plenefisch and Bonjer 1997; Cuenot et al. 2006; Meixner et al. 2014). The stress ratio is close to 1.0 for S_{Hmax}/S_v and 0.55 for S_{hmin}/S_v (Cornet et al. 2007; Valley and Evans 2007).

The Buntsandstein formation is, due to its high permeability, one of the preferred horizons for targeting hydrothermal reservoirs in the URG (Stober and Bucher 2014). Due to its polyphase tectonical history, the Buntsandstein is separated into different blocks with varying subsidence and exhumation (Ziegler et al. 2004). The depth of the Buntsandstein is 3000 m below surface in the central part of the URG with a thickness up to 500 m (Jodocy and Stober 2010). The temperature of the Buntsandstein reservoir is 160 °C with an elevated geothermal gradient of 45–50K km⁻¹ (Stober and Bucher 2014). Stresses between 35 and 75 MPa have been observed for the geothermal site of Soultz-sous-Forêts and are expected in the Buntsandstein reservoir (Cornet et al. 2007; Valley and Evans 2007). Analogs of the Buntsandstein are found in nearby outcrops, e.g., in the Vosges Mountains, the Kraichgau and the Black Forest (Eisbacher and Fielitz 2010; Bauer et al. 2015, 2017).

Mechanical characterization

Uniaxial and triaxial tests are common lab testing methods to assess the reservoir behavior under varying stress conditions (Fjar et al. 2008). These tests can provide information about static mechanical parameters (e.g., Poisson's ratio, Young's modulus, yield and failure stress) for a single sample under defined experimental conditions (Jaeger et al. 2007). The tests help to predict the volumetric changes due to compaction (Zoback 2011).

Data characterizing the mechanical properties of different kind of high porous sandstones are collected by the oil industry and can be found in Chang et al. (2006), Cuss et al. (2003) and Wong et al. (1997). Bauer et al. (2017) show the UCS, Young's modulus and porosities of Buntsandstein analogs from the eastern URG. Triaxial experiments on Triassic Sandstone of the Vosges (VsSst) have been reported by Bésuelle (2001).

It was shown that rocks in the upper crust are not very sensitive to temperature- and strain rate changes (Serdengecti and Boozer 1961; Donath and Fruth 1971). The main objectives are the prediction of failure under varying confining pressures, using different approaches and concepts. Different concepts can be used: (1) a linear correlation between the horizontal and vertical stresses, like Mohr–Coulomb and Drucker–Prager (Drucker and Prager 1952), or (2) specific failure envelope to describe mathematically

and empirically the behavior of different rock types. The latter approach is divided into two categories: brittle and compactive, depending on the failure or localization behavior. The volume of the sample increases in brittle failure, while it decreases for compaction (Rutter and Glover 2012). The gradual transition, between these two end members of failure types, is the subject of intensive scientific investigations aiming to understand the compaction behavior and the effects on mechanical parameters (e.g., Wong et al. 1997; Rudnicki 2004; Rutter and Glover 2012; Wong and Baud 2012). So, for practical purposes, usually an elliptical shaped failure surface is assumed (e.g., Baud et al. 2000; Rutter and Glover 2012). Instead, for brittle failure often a parabolic failure envelope is observed (e.g., Khan et al. 1991; Cuss et al. 2003). Rutter and Glover (2012) connect the transition to the critical state concept, where in differential vs. mean stress space, a linear relation with a slope of 1.18 ± 0.03 represents the transition, where no volume change at failure occurs.

The impact of the geomechanical behavior on hydraulic-related parameters, like porosity and permeability of the reservoir, is commonly known as poroelasticity (Terzaghi 1943; Biot 1956). The significance of mechanical and thermal variations to hydraulic parameters affecting the productivity of a reservoir is huge (Geertsma 1957; Zimmerman 2000; Bernabé et al. 2003), while their quantification with measurements is limited (Han and Dusseault 2003). The relationship between the two parameters porosity and permeability is in most cases described by a Kozeny–Carman-like relationship (Carman 1956).

Methods

Rock material

Two types of sandstone with different mineralogical composition have been used in the triaxial experiments: Pfinztal Sandstone (PfSst) and Tennenbach Sandstone (TenSst). Both rock types are analogs for the lower Triassic Buntsandstein formation in the Upper Rhine Graben (URG) and have been collected in quarries close to the URG. An extensive study on the petrological parameters is done by Schmidt et al. (2017).

Pfinztal Sandstone

The Pfinztal Sandstone (PfSst) is a red-colored, compact and well-sorted sandstone with a grain size between 0.04 and 0.2 mm, typically > 0.1 mm (Fig. 1a, b). The framework is based on angular and sub-spherical clasts and elongated muscovite plates which lead to a layered texture (Fig. 1a). The matrix is grain supported. The modal composition is 49% quartz, 16% K-feldspar, 11% muscovite, 15% cementation including hematite and 1% accessory phases (Table 1). The samples show slight alteration. The porosity is 8%, the permeability is $3.0 \cdot 10^{-17}$ m² (measured for four samples in permeameters) and the density is 2.38 g/cm³ (Schmidt et al. 2016).

Tennenbach Sandstone

The Tennenbach Sandstone (TenSst) is a red-colored, coarse-grained and well-sorted sandstone with a grain size under 0.5 mm (Fig. 1c, d). The clasts are well rounded mostly spherical. The modal composition of the samples is 83% quartz, 2% altered K-feldspar, 5% cementation (including hematite) and 1% accessory phases like mica (Table 1). The

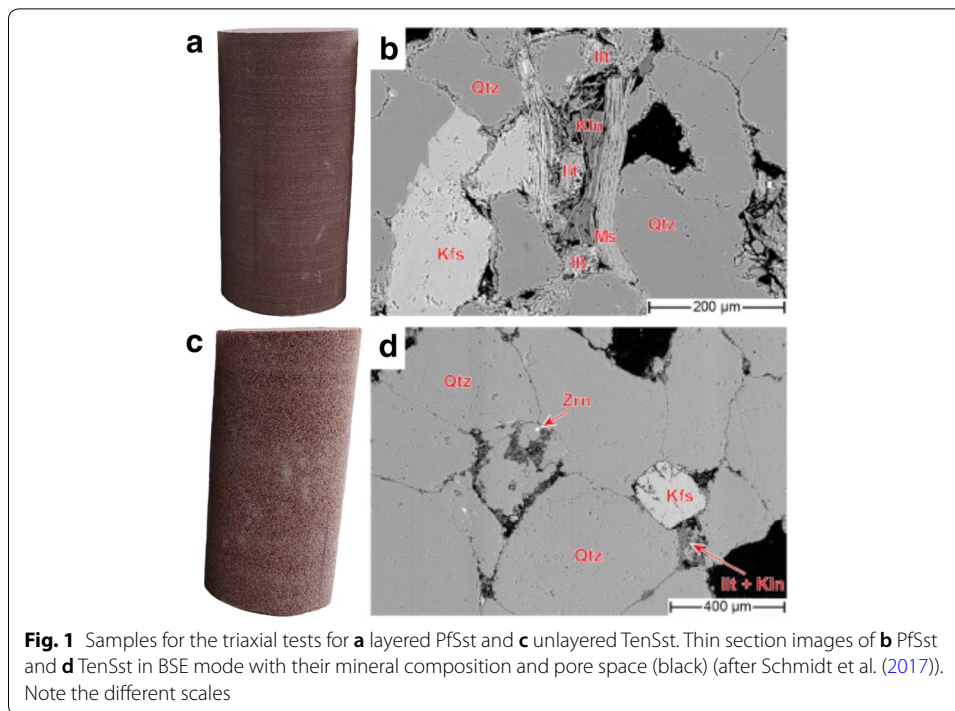


Table 1 Mineral composition of the two sandstone variations Pfnztal Sandstone and Tennenbach Sandstone used in the triaxial tests (Schmidt et al. 2017)

| In vol (%) | Pfnztal Sandstone | Tennenbach Sandstone |
|-------------|-------------------|----------------------|
| Quartz | 49 | 83 |
| K-feldspar | 16 | 2 |
| Muscovite | 11 | 0 |
| Cementation | 15 | 5 |
| Accessories | 1 | 1 |
| Pore space | 8 | 9 |

texture is grain supported, isotropic and without layering. The feldspar grains are significantly smaller than the quartz grains. The porosity is 9%, the permeability, as an average of four samples in permeameter measurements, is $4.0 \cdot 10^{-17} \text{ m}^2$ and the density is 2.13 g/cm^3 (Schmidt et al. 2016).

By comparing both sandstone types, we see differences in their petrological characterization. The Tennenbach Sandstone is more coarsely grained than the Pfnztal Sandstone, much more homogeneous and has a lower density (2.13 g/cm^3 against 2.38 g/cm^3). The amount of cementation, building the rock matrix, is significantly lower in Tennenbach Sandstone (5% against 15% in PfSst).

Triaxial tests

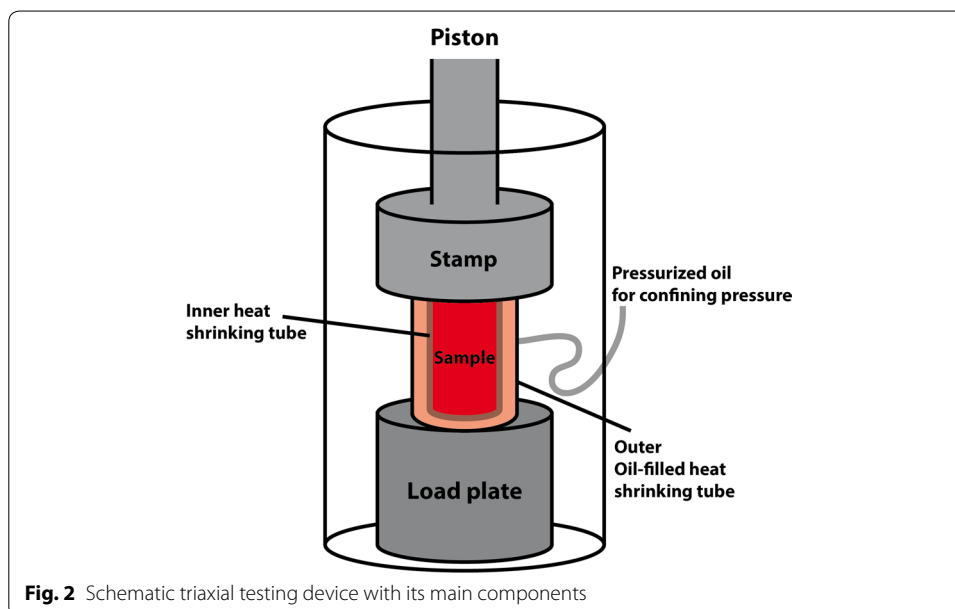
The triaxial testing system “Form + Test Alpha 2-3000 S” at the University of Freiburg was used for laboratory experiments. This triaxial cell has the ability to perform thermo-mechanical tests with dried samples. The maximum force is restricted to 3000 kN, which

is related to a maximum stress of 2387 MPa, by the hydraulic movement of a stamp on the top surface, while the bottom is fixed (Krietsch 2014). The confining pressure is applied through pressurized oil surrounding the specimen in an outer shrinking tube. The sample is sealed with an inner shrinking tube to prevent an interaction between oil and sample. The oil pressure can sustain a confining pressure of 150 MPa. Heating of the samples up to 200 °C is possible. Due to technical restrictions, the lateral stress or confining pressure is equal in every direction ($\sigma_1 = \sigma_2$). A schematic sketch is shown in Fig. 2.

Due to the findings of Cornet et al. (2007) and Valley and Evans (2007), the triaxial tests had to be carried out at least up to 75 MPa.

The samples, $n=11$ for PfSst and $n=12$ for TenSst, have cylindrical shape with a grinded bottom and top surface to reduce friction. The length:width ratio is 2:1 with a length of 80 mm and a diameter of 40 mm. The orientation of the loading axis is perpendicular with respect to the layering of the samples, especially for PfSst. Before conducting the experiments, the samples were dried. The deformation is applied at the top surface of the sample with a constant displacement rate of 1 mm/min, corresponding to $1.6 \cdot 10^{-5}$ m/s, until the specimen fails. Due to the scope of this study predicting reservoir conditions, experiments with constant confining pressures of 0, 50, 60, 70 and 90 MPa have been conducted for each type of sandstone. During the loading, the confining pressure is increased to the predefined limit and then kept constant during final axial loading of the specimen. The temperature is kept constant at room temperature of 20 °C during the changing confinement experiments. Additionally, we carried out triaxial tests with temperatures of 80 °C and 100 °C with a constant confinement of 50 MPa.

During the experiments, the averaged axial displacement and force on the upper surface of the sample and the confining pressure acting on the mantle are measured with an accuracy of 0.1 mm (displacement), 0.1 kN (force) and 0.1 bar (confinement). Due to device limitations, the stamp has a round shape with a diameter of 100 mm ($A_{\text{stamp}} = 0.00785 \text{ m}^2$),



which is larger than the sample size of 40 mm ($A_{\text{sample}}=0.00126 \text{ m}^2$) used in the study. Thus, the measured axial force has to be corrected by splitting in force acting on sample (F_{sample}) and force acting on confinement ($F_{\text{confinement}}$). The axial stress is corrected and calculated with Eq. 1:

$$\sigma_1 = \frac{((F_{\text{sample}} + F_{\text{confinement}}) - \sigma_3 * (A_{\text{stamp}} - A_{\text{sample}}))}{A_{\text{sample}}} \quad (1)$$

Due to the test performance, the axial stress is measured correctly when it exceeds the confining pressure ($\sigma_1 > \sigma_2$) and the force of the stamp is acting mainly on the sample. The material contrast between sample and stamp creates friction at the junction. This leads to an inhomogeneous stress distribution in the sample (Vutukuri et al. 1974). In the case of uniaxial testing ($\sigma_2 = \sigma_3 = 0$), it is possible to measure the lateral or radial deformation with an extensometer. The maximum strength, which the samples can reach with uniaxial setup, is called unconfined compressive strength (UCS). With known axial loading, radial and axial deformation, it is possible to calculate the elastic parameters of the rock samples, like Poisson ratio ν and Young's modulus E , using Hooke's law in the linear elastic part of the deformation (Jaeger et al. 2007).

Numerical methods

The numerical evaluation was carried out with the open-source software REDBACK (Poulet et al. 2016), which is based on the THMC-framework MOOSE (Multiphysics Object-Oriented Simulation Environment) (Gaston et al. 2009). MOOSE is a finite-element platform to solve multiphysical problems in an implicit and tightly coupled manner. It acts on unstructured and structured meshes and is highly scalable to work on powerful supercomputers in parallel architectures. The framework uses the finite-element libraries of LibMESH (Kirk et al. 2006) and PETSc solver (Balay et al. 2016). The implementation is done in a dimensionless form as single partial differential equations (PDEs). As every kernel is only solving for a single variable, it is possible to activate or deactivate specific parts of the code to focus on a single problem. The coupling is achieved through linking different variables and processes in an implicit or explicit way.

The application REDBACK (Rock mEchanics with Dissipative feedBACKs) is developed to solve thermo-hydro-mechanical problems in a dimensionless form (Poulet et al. 2016). It is based on the Tensor Mechanics module, which is provided by the MOOSE framework and extends it with additional constitutive models for the overstress plasticity, like von-Mises, Drucker–Prager or modified Cam-Clay (Poulet and Veveakis 2016).

Mechanical implementation

According to Perzyna (1966), the approach is based on the principles of overstress plasticity. The total strain rate can be divided in a reversible elastic ($\dot{\epsilon}_{ij}^{\text{el}}$) and an irreversible plastic (inelastic, $\dot{\epsilon}_{ij}^{\text{pl}}$) part (Eq. 2).

$$\dot{\epsilon}_{ij}^{\text{total}} = \dot{\epsilon}_{ij}^{\text{el}} + \dot{\epsilon}_{ij}^{\text{pl}} \quad (2)$$

In Eq. 3, the elastic deformation and effective stress tensor (σ') evolution follow a linear thermo-elastic law. The first term is the Hooke's law and the second one the volumetric stress triggered by volumetric thermal expansion (λ_s) initiated by temperature changes (ΔT). C_{ijkl} is the elasticity tensor. Since we are focusing on the effects of pressure changes and the samples have been in thermal equilibrium, the second term can be neglected.

$$\sigma'_{ij} = C_{ijkl} * \dot{\epsilon}_{kl}^{el} - \lambda_s * \frac{E}{1 - 2\nu} \Delta T \quad (3)$$

Note that the effective stress (σ'_{ij}) in Eq. 4, due to Terzaghi's principle, is a coupling between the absolute stress (σ_{ij}) and the pore pressure (P_f). The Biot's coefficient (α) takes the bulk modulus and the compressibility of the rock into account (Biot 1956).

$$\sigma'_{ij} = \sigma_{ij} - \alpha P_f \quad (4)$$

If a critical stress defined by the yield surface in the sample is reached, the deformation becomes irreversible and inelastic. The inelastic strain rate tensor can be split into volumetric ($\dot{\epsilon}_{vol}^{pl}$) and deviatoric ($\dot{\epsilon}_{dev}^{pl}$) deformation and follows an associative plastic flow-law (Poulet and Veveakis 2016) where the strain increment is normal to the yield surface (Eq. 5).

$$\dot{\epsilon}_{ij}^{pl} = \sqrt{\dot{\epsilon}_{dev}^{pl2} + \dot{\epsilon}_{vol}^{pl2}} * \frac{\partial f}{\partial \sigma'_{ij}} \quad (5)$$

The first part, bounded by the root, is a plastic multiplier and f the defined yield function which is related to the effective stresses. The deviatoric ($\dot{\epsilon}_{dev}^{pl}$) and volumetric ($\dot{\epsilon}_{vol}^{pl}$) strain rate tensor are calculated with Eqs. 6a and b.

$$\dot{\epsilon}_{dev}^{pl} = \dot{\epsilon}_0 * \left\langle \frac{q - q_y}{\sigma_{ref}} \right\rangle^m \quad (6a)$$

$$\dot{\epsilon}_{vol}^{pl} = \dot{\epsilon}_0 * \left\langle \frac{p' - p_y}{\sigma_{ref}} \right\rangle^m \quad (6b)$$

$\dot{\epsilon}_0$ is the reference strain rate, m is an exponent, q is the deviatoric stress, p' is the effective mean stress, q_y and p_y are the stresses at yield, while σ_{ref} is the reference stress. The Macaulay brackets in Eq. 6 ensure zero plastic deformation before touching the yield surface. During plastic deformation, the consumed energy or work can be decomposed in stored energy and dissipated energy (Chrysochoos et al. 1989). The related temperature change was observed mainly in metals (Johnson et al. 1964).

A Drucker–Prager (DP) yield envelope (Eq. 7) is used to numerically quantify the starting point of plastic deformation (Drucker and Prager 1952). This DP-criterion is a linear, time-independent and pressure-dependent criterion, where the deviatoric yield stress (q_y) is a function of the volumetric mean yield stress (p_y) with a given slope (M) and known initial yield stress (q_{y0}). These parameters are measurable with the conducted triaxial tests.

$$q_y = q_{y0} + p_y * M \quad (7)$$

Another empirical criterion for brittle behavior of porous medium type materials, like sandstone, was used by Khan et al. (1991) and applied to a wide range of different

sandstones by Wong et al. (1997) and Cuss et al. (2003). This criterion describes the relationship between differential and hydrostatic stress in brittle regimes as a parabola with a maximum reachable differential stress ($q_{y,max}$) and mean stress ($p_{y,max}$) (Eq. 8). When this maximum stress is reached, the samples will undergo compactive behavior until grain crushing occurs. Rutter and Glover (2012) take up this concept of changing behavior and refer the critical differential stress to linear increase with a slope of 1.18 ± 0.03 .

$$q_y = q_{y,max} - \left(\frac{q_{y,max}}{(1 - p_{y,max})^2} * (p_y - p_{y,max})^2 \right) \quad (8)$$

Coupled hydro-mechanical behavior

To evaluate the influence of stress and strain on porosity and permeability, a poroelastic approach is considered (Zimmerman 2000). The sample is treated as a porous medium with a solid skeleton and voids in between. The remaining porosity (φ) is defined as initial porosity (φ_0) and the changes of interconnected pore volume, related to mechanical deformation, elastic ($\Delta\varphi_{mech}^{el}$) and plastic ($\Delta\varphi_{mech}^{pl}$) (Eq. 9) (Poulet and Veveakis 2016).

$$\varphi = \varphi_0 + \Delta\varphi_{mech}^{el} + \Delta\varphi_{mech}^{pl} \quad (9)$$

With Eq. 10:

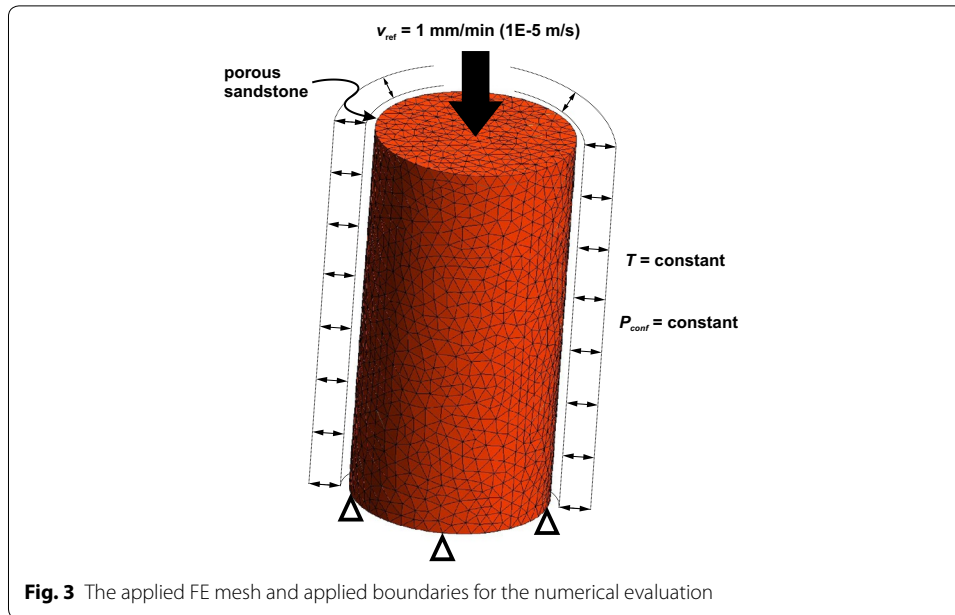
$$\Delta\varphi_{mech}^{el} = (1 - \varphi) * (\beta_s * \Delta P_f - \lambda_s * \Delta T + \Delta\epsilon_{vol}^{el}) \quad (10a)$$

$$\Delta\varphi_{mech}^{pl} = (1 - \varphi) * \Delta\epsilon_{vol}^{pl} \quad (10b)$$

where ($\beta_s * \Delta P_f$) is related to the compressibility of the solid due to pore pressure increase, ($\lambda_s * \Delta T$) the thermal expansion of the solid phase due to temperature increase and ($\Delta\epsilon_{vol}^{el}$) to elastic changes in the volume of the sample. ($\Delta\epsilon_{vol}^{pl}$) is the increment in volumetric plastic strain. Note that $\Delta\varphi_{mech}^{el}$ is typically negative in compressional regimes. No pore pressure or temperature changes are assumed, the changes in hydraulic-related rock parameters only depend on the volumetric change during deformation and the reduction of pore space.

Modeling

The 3D unstructured finite-element mesh is created in Gmsh (Geuzaine and Remacle 2017), representing a cylinder with a length:width ratio of 2:1. No artificial flaws or weak zones are added, to guarantee comparable results with the experiments carried out with the triaxial testing equipment. The modeling itself will be implemented in two steps. In the first step, the hydrostatic loading ($\sigma_1 = \sigma_2 = \sigma_3$) is applied to the sample. A Neumann boundary condition is acting on the mantle, bottom and top surfaces to apply a homogeneous stress field and resulting displacement of the whole mesh (Fig. 3). In the second step, the calculated displacements of the previous step are applied to the mesh as an initial condition. The bottom and top surfaces are constrained in x- and y-directions, the bottom additionally in the z-direction, to guarantee comparability to the experimental results. The upper boundary is displaced in the



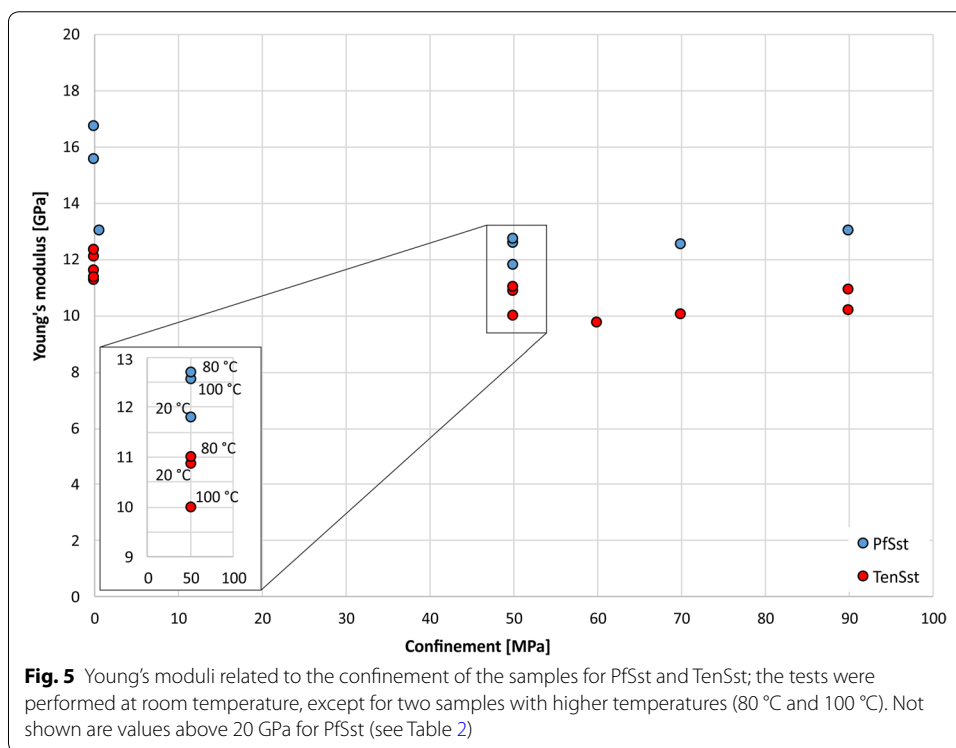
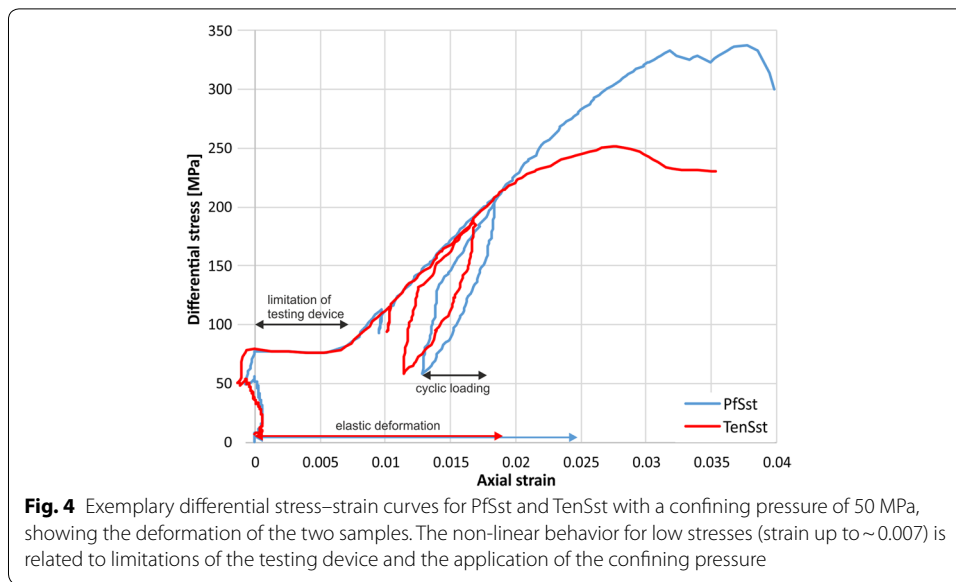
z-direction as a function of time in agreement with the triaxial experiments, while the stress acting on the lateral surface is kept constant. Since the focus is on the deformation processes and their coupled effects on sample and reservoir scale, the experimental results are averaged and used as constant input parameters for the numerical evaluation (Khajeh 2013; Settari et al. 2013).

Results

Triaxial tests

For both types of sandstone (Pfinztal and Tennenbach Sandstone), uniaxial and triaxial tests have been carried out. For the uniaxial tests, the axial and radial displacement and axial force were measured to calculate the Poisson's ratio and axial stress. The final Poisson's ratio is the average of at least five calculated values to decrease the uncertainty of natural inhomogeneities, which have a strong influence in unconfined samples. Thus, the Poisson's ratio for PfSst is 0.14 ± 0.03 and for TenSst 0.24 ± 0.04 . For the triaxial tests, the axial and radial force and axial displacement were measured to calculate the acting stresses. We focused our triaxial tests between 50 and 90 MPa due to reservoir conditions. Figure 4 shows selected stress–strain curves for a confining pressure of 50 MPa for TenSst and PfSst.

With known strain and stress in the linear elastic part of the deformation, the Young's modulus is calculated. Figure 5 and Table 2 show the experimental results for the samples of both sandstone types. Generally, the uniaxial tests lead to higher Young's moduli than the triaxial tests. Thus, for example, the Young's modulus for Pfinztal Sandstone is in the range between 12.5 and 26.4 GPa, while the mean value



for the confined samples is significantly lower (13.4 ± 1.5 GPa). The overall average of the Young's modulus of Tennenbach Sandstone is 10.9 ± 0.8 GPa. Most of the experiments were carried out at 20 °C. Two samples of both sandstones, with a confinement of 50 MPa, have been tested at 80 and 100 °C. These tests show similar Young's moduli without a significant visible influence of temperature (Fig. 5). The averaged results and their uncertainty are shown in Table 3. To calculate the

Table 2 Experimental data for PfSst and TenSst from uniaxial and triaxial experiments

| | Density (kg/m ³) | Confining pressure (MPa) | Maximum differential stress (MPa) | Young's modulus (GPa) | Poisson's ratio (-) | Temp (°C) |
|----------------------|------------------------------|--------------------------|-----------------------------------|-----------------------|---------------------|-----------|
| Pfinztal Sandstone | | | | | | |
| PfSst_10 | 2290 | 0 | – | 13.0 | 0.18 | 20 |
| PfSst_12 | 2400 | 0 | 114 | 16.7 | 0.12 | 20 |
| PfSst_13 | 2540 | 0 | 114 | 15.6 | 0.19 | 20 |
| PfSst_16 | 2460 | 0 | – | 25.7 | 0.14 | 20 |
| PfSst_17 | 2380 | 0 | – | 26.8 | 0.1 | 20 |
| PfSst_18 | 2380 | 0 | 142 | 26.4 | 0.11 | 20 |
| PfSst_11 | 2280 | 50 | 337 | 11.8 | – | 20 |
| PfSst_28 | 2430 | 50 | 352 | 12.6 | – | 100 |
| PfSst_29 | 2400 | 50 | 366 | 12.7 | – | 80 |
| PfSst_14 | 2320 | 70 | 433 | 12.5 | – | 20 |
| PfSst_15 | 2290 | 90 | 471 | 13.0 | – | 20 |
| Tennenbach Sandstone | | | | | | |
| TenSst_9 | 2020 | 0 | – | 12.1 | 0.23 | 20 |
| TenSst_11 | 2090 | 0 | 42 | 11.6 | 0.27 | 20 |
| TenSst_14 | 2250 | 0 | 46 | 11.3 | 0.2 | 20 |
| TenSst_15 | 2170 | 0 | 47 | 11.5 | 0.24 | 20 |
| TenSst_18 | 2170 | 0 | – | 12.4 | 0.28 | 20 |
| TenSst_13 | 2070 | 50 | 251 | 10.9 | – | 20 |
| TenSst_26 | 2070 | 50 | 256 | 10.0 | – | 100 |
| TenSst_27 | 2070 | 50 | 243 | 11.0 | – | 80 |
| TenSst_24 | 2190 | 60 | 282 | 9.7 | – | 20 |
| TenSst_16 | 2030 | 70 | 310 | 10.0 | – | 20 |
| TenSst_17 | 2030 | 90 | 332 | 10.2 | – | 20 |
| TenSst_28 | 2070 | 90 | 358 | 10.9 | – | 20 |

mechanical properties of the reservoir, the estimation of the maximum applicable stress until material failure occurs is necessary.

The comparison of the experimental results shows that the elastic modulus of the Pfinztal Sandstone is higher than the Tennenbach Sandstone (13.4 GPa compared to 10.9 GPa) (Table 3; Fig. 5). The unconfined compressive strength (UCS) and the slope of linear regression line between differential stress and mean stress are higher for PfSst, as well. Due to the higher Poisson's ratio, the effect of axial deformation on lateral deformation is higher in TenSst. The failure strength of both analogs shows a linear trend with increasing confinement with a slope of 1.80 (PfSst) and 1.63 (TenSst) (Fig. 7).

The results of the triaxial tests for PfSst and TenSst are summarized in Table 3 and have been applied to the numerical evaluation. The results of the triaxial tests show that at reservoir depth no mechanical failure is expected.

Numerical modeling

Maximum stress

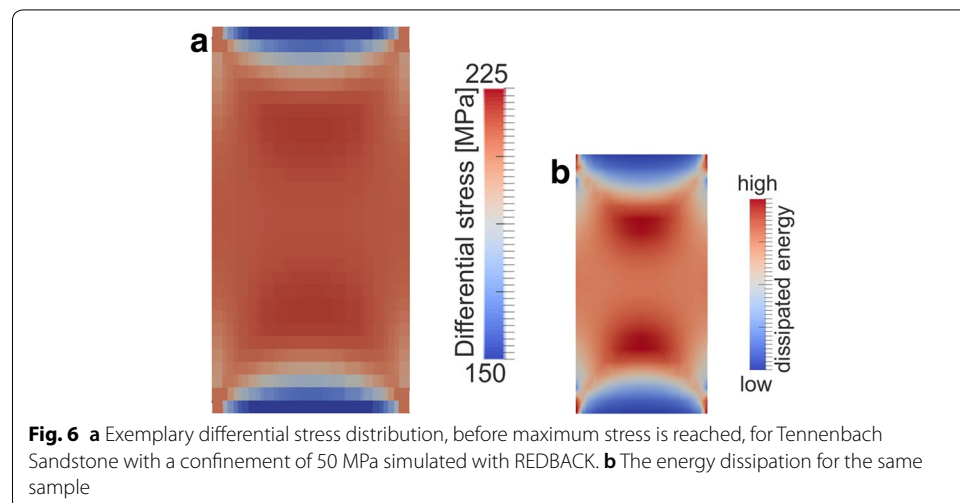
The mechanical properties, calculated from the results of the triaxial tests (Table 3), are used as input parameters for the numerical simulation. All input parameters are

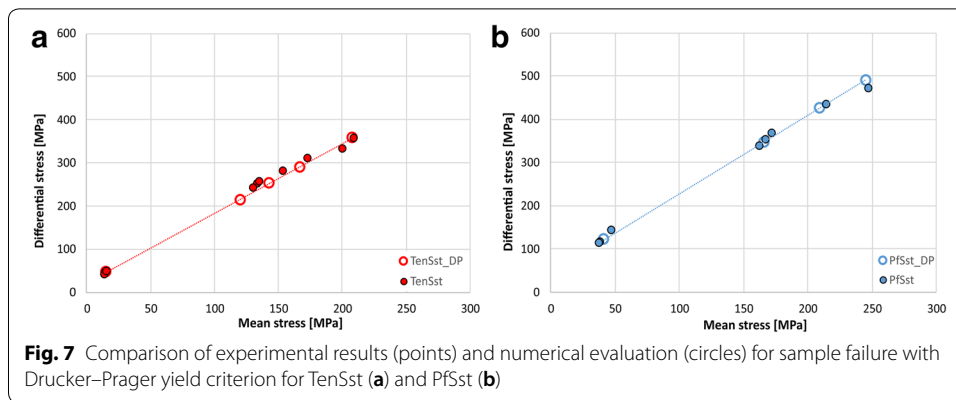
Table 3 Summary of the relevant data and uncertainty for PfsSt and TenSst

| | Pfintal Sandstone | Tennenbach Sandstone |
|------------------------------|------------------------|------------------------|
| Young's modulus (GPa) | 13.4 ± 1.5 | 10.9 ± 0.8 |
| Poisson ratio | 0.14 ± 0.03 | 0.24 ± 0.03 |
| Porosity (%) | 8 | 9 |
| Density (kg/m ³) | 2380 ± 77 | 2130 ± 110 |
| Initial yield stress (MPa) | 36.0 | 16.1 |
| Displacement at top (m/s) | 1.6 * 10 ⁻⁵ | 1.6 * 10 ⁻⁵ |
| Slope of the yield surface | 1.80 | 1.63 |
| Confinement (MPa) | 0–90 | 0–90 |

assumed to be constant, and natural heterogeneities are neglected. We used the elastic law and overstress plasticity described in Eqs. 2–5, to predict the maximum stress the reservoir rocks can withstand. The yield surface, where irreversible deformation starts, is determined with Eq. 7 and applied to the samples depending on the confining pressure. Due to modeling as FE mesh (Fig. 3), the stress distribution in the sample can be visualized. Stress maxima are visible along an “elongated cross”, which is a result of the constrained upper/lower boundary of the numerical sample and expected in the experiments as well (Vutukuri et al. 1974). Figure 6a shows exemplary the stress distribution in the sample Tennenbach Sandstone at a confining pressure of 50 MPa. Additionally, it is possible to show the qualitative amount of dissipated energy during irreversible deformation (Fig. 6b) leading to temperature increase, both not measureable in the triaxial experiments.

Figure 7 shows the comparison between the experimental and numerical results for Pfintal Sandstone and the Tennenbach Sandstone. The confining pressures are assumed to be identical. The modeling for 90 MPa seems to slightly overestimate the differential stress compared to the results in the experiment. Measured and calculated results are in good agreement with a maximum difference of 19 MPa.

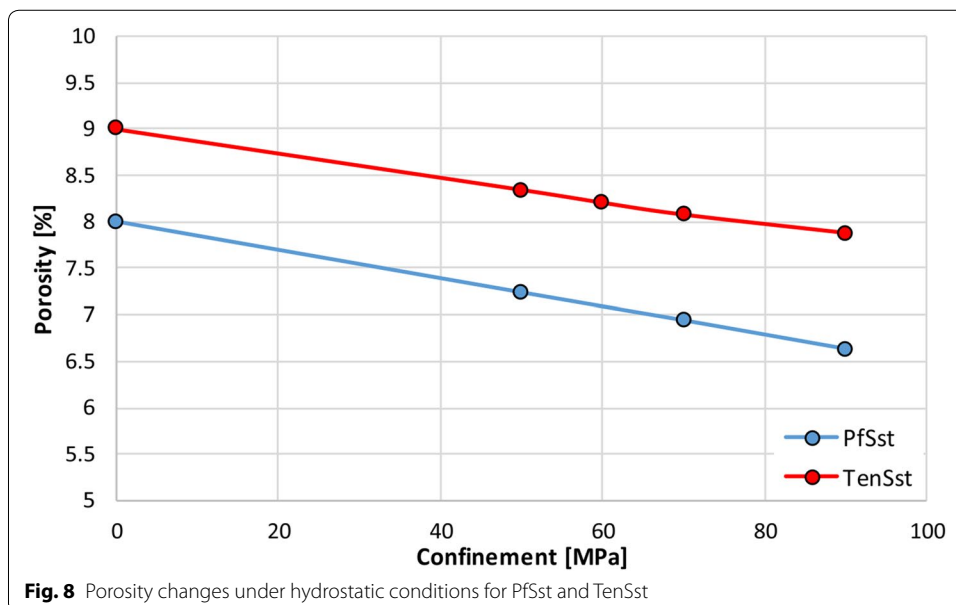


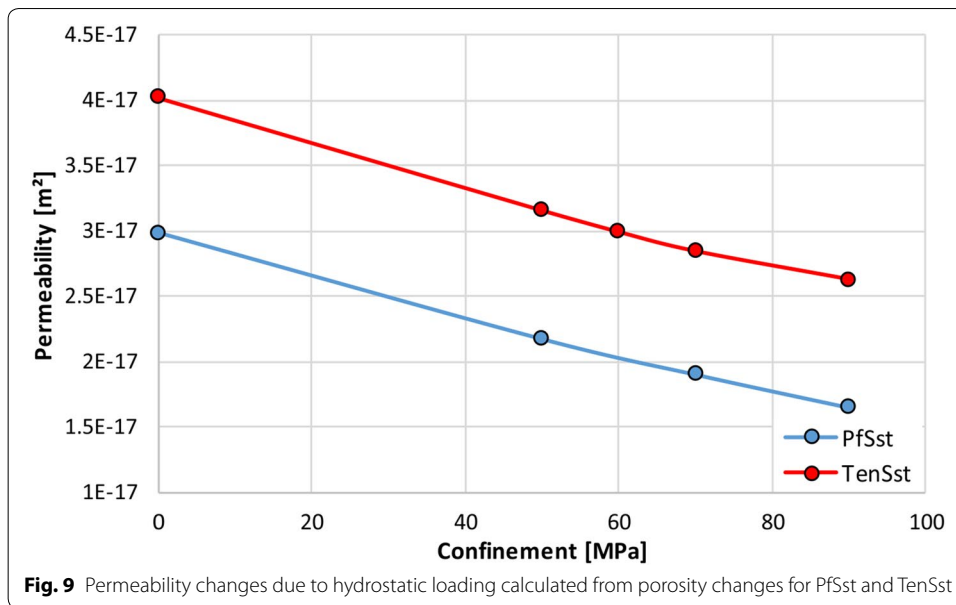


Impact on Poro-Perm relation

To calculate the hydraulic parameters as a result of mechanical deformation we use the initial confined modeling step with differential stress $q=0$ and $p = \sigma_1 = \sigma_2 = \sigma_3$, corresponding to hydrostatic conditions, expected in the reservoir. Porosity changes are related to volume changes in the sample, caused by volumetric deformation equally in the experiments and model. Thus, the hydrostatic compression has the most important influence on the remaining porosity. To calculate the porosity under these conditions, we used Eqs. 9 and 10. Figure 8 shows the remaining porosity depending on the confining pressure. Porosity decreases for PfSst from initially 8 to 6.6% at a circumferential stress of 90 MPa and for TenSst from 9 to 7.8% at 90 MPa.

Beside porosity, permeability is a key factor for evaluating the performance of a reservoir, e.g., for geothermal usage. It describes the transport of fluid and energy through the porous medium. To quantify the effect of porosity changes (φ) to permeability changes (k) the fundamental Kozeny–Carman relationship is used as a reference model (Carman 1956). More specific models and extensions to Kozeny–Carman, e.g., the fractal pore





space model for sedimentary rocks, have been developed to describe this relationship (Pape et al. 2000). With known initial porosity (φ_0) and initial permeability (k_0), this relationship can be expressed as Eq. 11 (Zoback 2011).

$$k = k_0 * \frac{(1 - \varphi_0)^2}{\varphi_0^3} * \frac{\varphi^3}{(1 - \varphi)^2} \quad (11)$$

Figure 9 shows the permeability evolution of Pfnzstal and Tennenbach Sandstone. The values are related to the changes in porosity. The permeability decreases for PfSst from initially $3.0 * 10^{-17}$ to $1.6 * 10^{-17}$ m² for a hydrostatic stress of 90 MPa and TenSst from initially $4.0 * 10^{-17}$ to $2.6 * 10^{-17}$ m².

Discussion

Triaxial experiments and numerical modeling

The static Young's moduli of the different sandstone types are shown in Fig. 5. The scattering of the unconfined Young's modulus for the PfSst (between 13 and 25 GPa) is related to material heterogeneities like initial microcracks, grain size, cementation and porosity differences between the different samples and the testing device itself (Dunn et al. 1973; Palchik 1999). The impact of these heterogeneities and flaws decreases with increasing confining pressure since a preconsolidation of the sample is applied with the confinement step (e.g., Zoback 2011). Additionally, the part of linear elasticity is limited in uniaxial tests which leads to a higher uncertainty in the evaluation of the mechanical parameters compared to triaxial tests with higher absolute strains. The average values of PfSst (13.4 GPa) and TenSst (10.9 GPa) are comparable with measurements from other sandstone types (Wong et al. 1997; Cuss et al. 2003). The majority of these values are in the range of 0–30 GPa, with some scattering to 74 GPa. The Young's modulus of Vosges Sandstone is calculated using the slope of the stress–strain ratio (linear part).

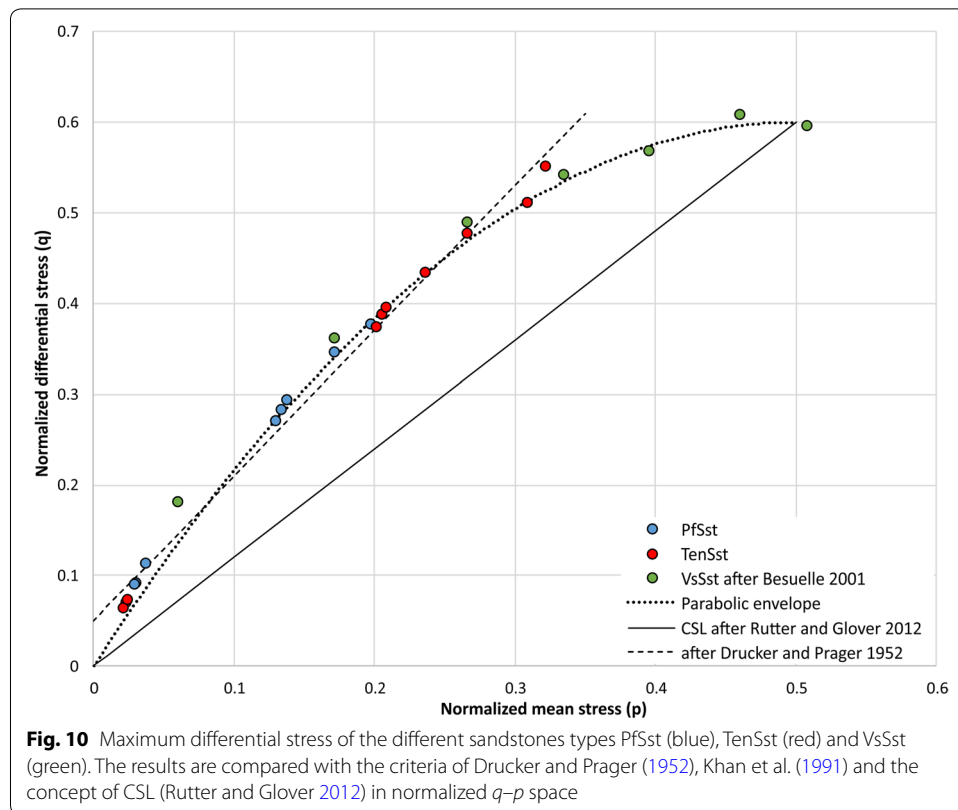
It is in the range of 12–13 GPa (Bésuelle 2001). Chang et al. (2006) have shown that Young's modulus and UCS reduce with increasing porosity. The porosity for the Buntsandstein probes used in this study is low (PfSst 8% and TenSst 9%) compared to other reservoir sandstones (>10%) (Chang et al. 2006) but fits with data reported by Bauer et al. (2017) for Buntsandstein analogs. To predict the failure, calculating the UCS, as initial failure strength under uniaxial loading, is important. The data in Chang et al. (2006) show indeed a positive correlation between Young's modulus and UCS for 260 sandstone samples, but a large variety of value pairs is observed and no precise trend is visible. However, the data of Chang et al. (2006) are in accordance with our samples of PfSst (123 MPa), TenSst (46 MPa) and VsSst (35 MPa), as well. Bauer et al. (2017) report UCS values in the range of 80–100 MPa for the Buntsandstein in the northeast URG.

The mechanical parameters for both investigated sandstones (Young's modulus and failure strength) show no measurable dependency on temperature up to 100 °C (Figs. 5, 7). This agrees with the findings of Ranjith et al. (2012) and Serdengecti and Boozer (1961), who demonstrate temperature sensitivity to be observed only for temperatures above 400 °C.

Failure stress prediction

We compare the results of our triaxial tests on TenSst and PfSst samples with the linear criterion of Drucker and Prager (1952) (Eq. 7), the parabolic envelope Khan et al. (1991) used for brittle failure (Eq. 8) and the critical state line of Rutter and Glover (2012) with a slope of 1.2, to find the best criterion for inter- and extrapolation to simulate reservoir conditions. Figure 10 shows the results and the comparison in the normalized q - p space. The normalization is applied with respect to a grain crushing pressure p^* , which is a function of *porosity * grain radius*, presented by Rutter and Glover (2012) and Zhang et al. (1990). High grain sizes reduce the potential maximum stresses, which are commonly known as Hall–Petch relationship (Chokshi et al. 1989). Additionally, the data of Bésuelle (2001) of the Vosges Sandstone (VsSst) are presented in Fig. 10. They show a reasonable fit with a maximum difference of 0.04 to the parabolic criterion used by Khan et al. (1991) with a maximum of $p=0.5$ and $q=0.6$. The results of TenSst and PfSst correspond well with both (linear and parabolic) criteria up to a normalized mean stress of 0.3. The linear plot is averaged through both sample types with a slope of 1.6 and an initial normalized differential stress of 0.05. The data points for the confined samples of TenSst are closer to the maximum differential strength of this sample type which results in a lower maximum stress resistivity.

The parabolic envelope used by Khan et al. (1991) starting at $x/y=0/0$ in the coordinate system's origin underestimates the failure strength for low confining pressures of both sandstone samples. The accuracy for differential stress prediction is in the range of possible reservoir stresses, between 50 and 80 MPa, 0.02 for normalized differential stress, while a slight overestimation of the maximum failure strength is possible. For higher confining pressures, at which the expected transition from brittle to compactive failure takes place, no data are available. Nevertheless, these absolute stresses are out of range for a possible URG reservoir as described in the geological overview. The expected failure stress for the criterion of Drucker and Prager (1952) fits well for normalized mean



stresses up to $0.27 (\pm 0.03)$ or absolute 210 MPa for TenSst and PfSst in both triaxial experiments and modeling (Fig. 7).

Hydraulic implications

The porosity and permeability of Tennenbach and Pfinztal Sandstone have been quantified in advance by thin section and permeability tests. REDBACK allows the coupling of mechanical deformation with hydraulic feedback. Thus, it is possible to quantify the porosity and permeability changes due to compressive loading and volumetric changes using Eqs. 9–11. The results are shown in Figs. 8 and 9. Porosity is decreasing from initially 8% to 6.6% (PfSst) and from 9% to 7.8% (TenSst), corresponding to a total reduction of 17.5% and 13.3%, respectively. The permeability decreases from $3.0 \cdot 10^{-17}$ to $1.6 \cdot 10^{-17} \text{ m}^2$ (PfSst) and from $4.0 \cdot 10^{-17}$ to $2.6 \cdot 10^{-17} \text{ m}^2$ (TenSst), which is a drop of 46.6% and 35%, respectively.

The Kozeny–Carman equation depends on different parameters of the pore geometry like a geometric factor, tortuosity and surface area, and assumes steady laminar flow. However, the calculation of the exact value is rather complex because the surface area, as the most relevant factor, is typically unknown. Equation 11 assumes a bed of spheres with fully interconnected pores and a constant geometric factor (Hassanzadegan and Zimmermann 2014), while changes in pore deformation and connection have been neglected.

Effects on upscaling

The extrapolation and upscaling of the results to reservoir conditions is limited to a certain extent related to the samples, experiments, modeling approach and to the reservoir itself, as described below. Experiments and modeling assume fully dry conditions, while a geothermal reservoir is saturated under hydrostatic or sometimes even over-pressure conditions. Positive changes in pore pressure, for example caused by fluid injection or compaction, would increase the porosity in the sphere of influence related to Eq. 9 and decrease the effective stress acting on the sample (Biot 1956). On the other hand, a decrease in temperature, for example by cold water injection, will increase the porosity as well due to volume reduction of the solid phase (Eq. 9). A generalization was made in terms of hydrostatic stress conditions because the poly-axial behavior is unknown, but it could lead to changes in stress distribution. Taking these considerations into account, a lower decrease of porosity and permeability in the reservoir is expected.

The scale of the sample in triaxial tests is limited due to technical reasons. The internal setup of the large-scale reservoir is typically unknown, containing material heterogeneities as well as faults and fractures. For the numerical evaluation, we assumed a homogeneous and non-fractured sandstone body for comparison reasons with analog studies (triaxial tests). This assumption is limited since first of all, the sedimentary rocks of the URG have strongly varying facies (Bauer et al. 2017), leading to a substantial heterogeneity in the mechanical parameters, like UCS. Values between 35 and 123 MPa are reported for the Buntsandstein. Additionally, due to the deformation history of the URG, the Buntsandstein is characterized by various fault and fracture networks, affecting the mechanical and hydraulic parameters of the reservoir rock (Meixner et al. 2014). It is commonly assumed that rocks in the vicinity of fractures have no or strongly reduced cohesion (Jaeger et al. 2007), leading to a lower stress resistance. Vutukuri et al. (1974) reported that the rock strength is mainly affected by the largest crack. A larger sample or reservoir may have larger cracks, leading to a decrease in overall rock strength. So, the results tend to overestimate the resistivity of the reservoir rock (Chang et al. 2006).

On the other hand, fractures affect the permeability and porosity of the reservoir directly (Stober and Bucher 2014), while the matrix is acting more or less as a storage. Thus, fractures are preferable pathways for fluids when critical stresses are observed and dilatancy or shear displacement take place (Barton et al. 1995). The permeameter measurements ($4.0 \cdot 10^{-17} \text{ m}^2$ and $3.0 \cdot 10^{-17} \text{ m}^2$, respectively) are in good accordance with the relatively small values derived by core samples of the Buntsandstein (Stober and Bucher 2014). As described before, the permeability is a combination of matrix and fractures. Stober and Bucher (2014) reported an averaged formation permeability of $5 \cdot 10^{-15} \text{ m}^2$. Analogs of the eastern border of the URG show comparable matrix porosities between 3 and 8% (Bauer et al. 2017). On the other hand, alteration, like remineralization and precipitation of new minerals along fractures, can decrease the fracture permeability (Stober and Bucher 2014; Schmidt et al. 2017). Therefore, the chances of successful upscaling results from analog studies to reservoir conditions are higher for formations with less complex internal structures like sedimentary basins, where porous media flow is the dominant process for transporting energy.

Summary and conclusions

By means of triaxial tests realized on analog rocks of the Buntsandstein formation of the URG, it is possible to predict the mechanical behavior of a possible geothermal reservoir rock under deformation in a general way. Two different types of Buntsandstein analogs, Tennenbach and Pfinztal Sandstone, have been investigated for mechanical and hydraulic characterization. Hydraulic tests show a low natural porosity of 9% (TenSst) and 8% (PfSst) and a permeability of $4.0 \cdot 10^{-17} \text{ m}^2$ (TenSst) and $3.0 \cdot 10^{-17} \text{ m}^2$ (PfSst). The Young's moduli, determined with the aid of triaxial tests, are in the range of 11–13 GPa and the Poisson's ratio is 0.24 (TenSst) and 0.14 (PfSst).

Uniaxial and triaxial tests were conducted to gain information concerning their geomechanical behavior under in situ conditions. For the triaxial tests, the confining pressure for every setup was kept constant between 50 and 90 MPa at room temperatures and additionally for a confining pressure of 50 MPa at temperatures of 80 and 100 °C. The experiments showed that an increase in horizontal stress, as confining pressure, leads to higher maximum stresses on the vertical axis. The maximum differential stress at a confining pressure of 90 MPa is 358 MPa (TenSst) and 471 MPa (PfSst). An influence of temperature was not visible. The measured stresses have been compared to different kinds of failure criteria to predict failure stress and for interpolation purposes. The rock-dependent parabolic failure envelope used by Khan et al. (1991) and the general criteria of Drucker and Prager (1952) are in good agreement with the triaxial experiments of TenSst and PfSst in the conducted stress regime expected in the URG (Fig. 10). For the weaker VsSst, the Drucker–Prager criterion leads to a strong overestimation of the maximum reachable stress (Fig. 10). The high stress resistivity of TenSst and PfSst to vertical stresses under confinement suggests that the rocks are in the elastic range of deformation in the Buntsandstein horizon.

Numerical modeling of the triaxial tests with the MOOSE framework allows us to have a look inside the rock sample and to quantify the stress maxima not homogeneously located within the specimen. Stress- and deformation-induced volume changes lead to void space reduction preferentially along the zone of increased deformation. With known initial porosity and permeability (hydraulic tests with a permeameter) and the change in porosity (calculated in the numerical model), the change in matrix permeability can be evaluated using a Kozeny–Carman relationship. Thus, the porosity is reduced to 7.8% (TenSst) and 6.6% (PfSst) and the permeability to $2.6 \cdot 10^{-17} \text{ m}^2$ (TenSst) and $1.6 \cdot 10^{-17} \text{ m}^2$ (PfSst), applying an isotropic stress of 90 MPa to the sample. This corresponds to a drop in permeability of 46.6% (PfSst) and 35% (TenSst) respectively. Measurements of these parameters during deformation and after failure can help to verify these results and decrease the uncertainty related to the approach applied.

For complex geological structures, like the fault-related Buntsandstein reservoir in the Upper Rhine Graben, large uncertainties in predicting the mechanical and hydraulic behavior are expected. Fault and fracture architecture can affect the hydraulic characteristics by improving or inhibiting fluid flow, depending on the interaction of different factors, e.g., lithology, displacement, temperature or time (Caine et al. 1996). Thus, it is necessary to investigate the mechanical behavior of reservoir rocks in the vicinity and within fault and damage zones when natural or artificial changes in the effective stress field occur. On the other hand, for more homogenous reservoirs, like sedimentary

basins, our results can provide an increased knowledge of the target horizon with higher accuracy.

The benefit of numerically modeling the triaxial tests is the possibility to pinpoint, quantify and separate the various processes which take place during deformation in the sample and on the boundaries in a scale-independent manner. This promotes an understanding of how different parameters, like UCS, Young's modulus or Poisson's ratio, affect the mechanical behavior on a smaller as well as on reservoir engineering scale. We can use these mechanical implications to evaluate the influence of natural and artificial stress changes, e.g., in the vicinity of wells, on hydraulic-related parameters, like permeability and porosity. In general, our results can help to fill the gap between borehole data and their transferability to reservoir scale.

Authors' contributions

RE evaluated the triaxial tests, performed the numerical modeling and wrote the manuscript. RS and IS helped to conduct the triaxial experiments. TK provided valuable support in the numerical modeling. IS and RE drafted the manuscript. IS supervised the research and finalization of the manuscript. All authors read and approved the final manuscript.

Acknowledgements

This study is part of the project "GeoFaces" supported by the Federal Ministry for Economic Affairs and Energy (BMWi) (No. 0324025C). Special thanks to Prof. Dr. T. Kenkmann and Hannes Kriesch (both University of Freiburg), which helped to conduct the experimental results. Special thanks to Dr. Max Peters, who introduced into the MOOSE framework. Particular thanks to the two anonymous reviewers, which helped to improve the quality of the paper.

Competing interests

The authors declare that they have no competing interests.

Availability of data and materials

All data analyzed in this study are presented in the manuscript.

Consent for publication

Not applicable.

Ethics approval and consent to participate

Not applicable.

Funding

The study is funded through the Federal Ministry for Economic Affairs and Energy (BMWi).

Publisher's Note

Springer Nature remains neutral with regard to jurisdictional claims in published maps and institutional affiliations.

Received: 17 May 2018 Accepted: 22 October 2018

Published online: 03 November 2018

References

- Agemar T, Brunken J, Jodocy M, Schellschmidt R, Schulz R, Stober I. Subsurface temperatures in Baden-Württemberg, Germany. *Zeitschrift der Deutschen Gesellschaft für Geowissenschaften*. 2013;164:49–62. <https://doi.org/10.1127/1860-1804/2013/0010>.
- Agemar T, Alten J-A, Ganz B, Kuder J, Kühne K, Schumacher S, Schulz R. The geothermal information system for Germany—GeotIS. *Zeitschrift der Deutschen Gesellschaft für Geowissenschaften*. 2014;165:129–44. <https://doi.org/10.1127/1860-1804/2014/0060>.
- Balay S, Abhyankar S, Adams M, Brown J, Brune P, Buschelman K, Dalcin L, Eijkhout V, Gropp W, Karpeyev D, Kaushik D, Knepley M, Curfman McInnes L, Rupp K, Smith B, Zampini S, Zhang H. PETSc user manual, Technical Report ANL-95/11—Revision 3.7. Argonne National Laboratory. 2016.
- Barton CA, Zoback MD, Moos D. Fluid flow along potentially active faults in crystalline rock. *Geol*. 1995;23:683. [https://doi.org/10.1130/0091-7613\(1995\)023%3c0683:FFAPAF%3e2.3.CO;2](https://doi.org/10.1130/0091-7613(1995)023%3c0683:FFAPAF%3e2.3.CO;2).
- Baud P, Zhu W, T-F Wong. Failure mode and weakening effect of water on sandstone. *J Geophys Res*. 2000;105:16371–89. <https://doi.org/10.1029/2000JB900087>.
- Bauer JF, Meier S, Philipp SL. Architecture, fracture system, mechanical properties and permeability structure of a fault zone in Lower Triassic sandstone, Upper Rhine Graben. *Tectonophysics*. 2015;647–648:132–45. <https://doi.org/10.1016/j.tecto.2015.02.014>.

- Bauer JF, Krumbholz M, Meier S, Tanner DC. Predictability of properties of a fractured geothermal reservoir: the opportunities and limitations of an outcrop analogue study. *Geotherm Energy*. 2017;5:65. <https://doi.org/10.1186/s40517-017-0081-0>.
- Bernabé Y, Mok U, Evans B. Permeability–porosity relationships in rocks subjected to various evolution processes. *Pure Appl Geophys*. 2003;160:937–60. <https://doi.org/10.1007/PL00012574>.
- Bésuelle P. Evolution of strain localisation with stress in a sandstone: brittle and semi-brittle regimes. *Phys Chem Earth Part A*. 2001;26:101–6. [https://doi.org/10.1016/S1464-1895\(01\)00032-1](https://doi.org/10.1016/S1464-1895(01)00032-1).
- Biot MA. General solutions of the equations of elasticity and consolidation for a porous material. *J Appl Mech*. 1956;23:91–6.
- Caine JS, Evans JP, Forster CB. Fault zone architecture and permeability structure. *Geol*. 1996;24:1025. [https://doi.org/10.1130/0091-7613\(1996\)024%3c1025:FZAAPS%3e2.3.CO;2](https://doi.org/10.1130/0091-7613(1996)024%3c1025:FZAAPS%3e2.3.CO;2).
- Carman P. Flow of gases through porous media. London: Butterworths Scientific Publications; 1956.
- Chang C, Zoback MD, Khaksar A. Empirical relations between rock strength and physical properties in sedimentary rocks. *J Pet Sci Eng*. 2006;51:223–37. <https://doi.org/10.1016/j.petrol.2006.01.003>.
- Chokshi AH, Rosen A, Karch J, Gleiter H. On the validity of the hall-petch relationship in nanocrystalline materials. *Scr Metall*. 1989;23:1679–83. [https://doi.org/10.1016/0036-9748\(89\)90342-6](https://doi.org/10.1016/0036-9748(89)90342-6).
- Chrysochoos A, Maisonneuve O, Martin G, Caumon H, Chezeaux JC. Plastic and dissipated work and stored energy. *Nucl Eng Des*. 1989;114:323–33. [https://doi.org/10.1016/0029-5493\(89\)90110-6](https://doi.org/10.1016/0029-5493(89)90110-6).
- Cornet FH, Bérard T, Bourouis S. How close to failure is a granite rock mass at a 5 km depth? *Int J Rock Mech Min Sci*. 2007;44:47–66. <https://doi.org/10.1016/j.ijrmmms.2006.04.008>.
- Cuenot N, Charléty J, Dorbath L, Haessler H. Faulting mechanisms and stress regime at the European HDR site of Soultz-sous-Forêts, France. *Geothermics*. 2006;35:561–75. <https://doi.org/10.1016/j.geothermics.2006.11.007>.
- Cuss RJ, Rutter EH, Holloway RF. The application of critical state soil mechanics to the mechanical behaviour of porous sandstones. *Int J Rock Mech Min Sci*. 2003;40:847–62. [https://doi.org/10.1016/S1365-1609\(03\)00053-4](https://doi.org/10.1016/S1365-1609(03)00053-4).
- Dunn DE, LaFountain LJ, Jackson RE. Porosity dependence and mechanism of brittle fracture in sandstones. *J Geophys Res*. 1973;78:2403–17. <https://doi.org/10.1029/JB078i014p02403>.
- Donath FA, Fruth LS. Dependence of strain-rate effects on deformation mechanism and rock type. *J Geol*. 1971;79:347–71. <https://doi.org/10.1086/627630>.
- Drucker DC, Prager W. Soil mechanics and plastic analysis or limit design. *Quart Appl Math*. 1952;10:157–65. <https://doi.org/10.1090/qam/48291>.
- Eisbacher GH, Fielitz W. Karlsruhe und seine Region: Nordschwarzwald, Kraichgau, Neckartal, Oberrhein-Graben, Pfälzerwald und westliche Schwäbische Alb. Sammlung geologischer Führer, vol. 103. Stuttgart: Borntraeger; 2010.
- Fitch PJR, Lovell MA, Davies SJ, Pritchard T, Harvey PK. An integrated and quantitative approach to petrophysical heterogeneity. *Mar Pet Geol*. 2015;63:82–96. <https://doi.org/10.1016/j.marpetgeo.2015.02.014>.
- Fjar E, Holt RM, Raaen AM. Petroleum related rock mechanics, 2nd ed. 2. Aufl. Developments in petroleum science, vol. 53. Elsevier professional, s.l. 2008.
- Gaston D, Newman C, Hansen G, Lebrun-Grandié D. MOOSE: a parallel computational framework for coupled systems of nonlinear equations. *Nucl Eng Des*. 2009;239:1768–78. <https://doi.org/10.1016/j.nucengdes.2009.05.021>.
- Geertsma J. The effect of fluid decline on volumetric changes of porous rocks. *Petrol Trans AIME*. 1957;210:331–40.
- Geuzaine C, Remacle J-F. Gmsh reference manual: the documentation for Gmsh 2.16. 2017.
- Grimmer JC, Ritter JRR, Eisbacher GH, Fielitz W. The Late Variscan control on the location and asymmetry of the Upper Rhine Graben. *Int J Earth Sci*. 2017;106:827–53. <https://doi.org/10.1007/s00531-016-1336-x>.
- Han G, Dusseault MB. Description of fluid flow around a wellbore with stress-dependent porosity and permeability. *J Pet Sci Eng*. 2003;40:1–16. [https://doi.org/10.1016/S0920-4105\(03\)00047-0](https://doi.org/10.1016/S0920-4105(03)00047-0).
- Hassanzadegan A, Zimmermann G. A poroelastic description of permeability evolution. *Pure Appl Geophys*. 2014;171:1187–201. <https://doi.org/10.1007/s00024-013-0714-6>.
- Held S, Genter A, Kohl T, Kölbl T, Sausse J, Schoenball M. Economic evaluation of geothermal reservoir performance through modeling the complexity of the operating EGS in Soultz-sous-Forêts. *Geothermics*. 2014;51:270–80. <https://doi.org/10.1016/j.geothermics.2014.01.016>.
- Illies JH. Bauplan und Baugeschichte des Oberrheingrabens. *Oberrhein Geol Abh*. 1965;14:1–54.
- Illies JH. The Rhine graben rift system-plate tectonics and transform faulting. *Geophys Surv*. 1972;1:27–60. <https://doi.org/10.1007/BF01449550>.
- Jaeger JC, Cook NGW, Zimmerman RW. Fundamentals of rock mechanics. 4th ed. Malden Mass: Blackwell Publ; 2007.
- Jodocy M, Stober I. Geologisch-geothermische Tiefenprofile für den baden-württembergischen Teil des nördlichen und mittleren Oberrheingrabens. *Erdöl Erdgas Kohle*. 2010;126:68–76.
- Johnson W, Baraya GL, Slater RAC. On heat lines or lines of thermal discontinuity. *Int J Mech Sci*. 1964;6:409–IN4. [https://doi.org/10.1016/s0020-7403\(64\)80001-1](https://doi.org/10.1016/s0020-7403(64)80001-1).
- Khajeh MM. Heterogeneity consideration and upscaling of elastic properties in coupled geomechanical flow simulation of SAGD. Dissertation. University of Alberta, Kanada. 2013.
- Khan AS, Xiang Y, Huang S. Behavior of Berea sandstone under confining pressure part I: yield and failure surfaces, and nonlinear elastic response. *Int J Plast*. 1991;7:607–24. [https://doi.org/10.1016/0749-6419\(91\)90046-2](https://doi.org/10.1016/0749-6419(91)90046-2).
- Kirk BS, Peterson JW, Stogner RH, Carey GF. libMesh: a C++ library for parallel adaptive mesh refinement/coarsening simulations. *Eng Comput*. 2006;22:237–54. <https://doi.org/10.1007/s00366-006-0049-3>.
- Kohl T, Hopkirk RJ. “FRACure”—a simulation code for forced fluid flow and transport in fractured, porous rock. *Geothermics*. 1995;24:333–43. [https://doi.org/10.1016/0375-6505\(95\)00012-F](https://doi.org/10.1016/0375-6505(95)00012-F).
- Krietsch H. Analysis of fracture topographies of deformed rocks using white light interferometry. Master thesis. Albert-Ludwigs-University, Freiburg. 2014.
- Lama RD, Vutukuri VS. Handbook on mechanical properties of rocks: testing techniques and results, 1. print. vol. 2, no. 1. Clausthal: Trans Tech Publications. 1978.
- Mansfield CS, Cartwright JA. High resolution fault displacement mapping from three-dimensional seismic data: evidence for dip linkage during fault growth. *J Struct Geol*. 1996;18:249–63. [https://doi.org/10.1016/S0191-8141\(96\)80048-4](https://doi.org/10.1016/S0191-8141(96)80048-4).

- Meixner J, Schill E, Gaucher E, Kohl T. Inferring the in situ stress regime in deep sediments: an example from the Bruchsal geothermal site. *Geotherm Energy*. 2014;2:233. <https://doi.org/10.1186/s40517-014-0007-z>.
- O'Sullivan MJ, Pruess K, Lippmann MJ. State of the art of geothermal reservoir simulation. *Geothermics*. 2001;30:395–429. [https://doi.org/10.1016/S0375-6505\(01\)00005-0](https://doi.org/10.1016/S0375-6505(01)00005-0).
- Palchik V. Influence of porosity and elastic modulus on uniaxial compressive strength in soft brittle porous sandstones. *Rock Mech Rock Eng*. 1999;32:303–9. <https://doi.org/10.1007/s006030050050>.
- Pape H, Clauser C, Iffland J. Variation of permeability with porosity in sandstone diagenesis interpreted with a fractal pore space model. *Pure Appl Geophys*. 2000;157:603–19. <https://doi.org/10.1007/PL00001110>.
- Perzyna P. Fundamental problems in viscoplasticity. In: Chernyi GG, editor. *Advances in applied mechanics*, vol. 9. New York: Academic Press; 1966. p. 243–377.
- Pflug R. *Bau und Entwicklung des Oberrheingrabens*. Darmstadt: Wissenschaftliche Buchgesellschaft; 1982.
- Philipp SL, Reyner D, Meier S, Hemes S, Hoffmann S, Lunsdorf NK, Oelrich ARI. Strukturgeologische Geländestudien in Aufschlussanalogien und Permeabilitätsentwicklung in geothermischen Reservoiren. *Geotecton Res*. 2008;95:137–9. <https://doi.org/10.1127/1864-5658/08/9501-0137>.
- Plenefisch T, Bonjer K-P. The stress field in the Rhine Graben area inferred from earthquake focal mechanisms and estimation of frictional parameters. *Tectonophysics*. 1997;275:71–97. [https://doi.org/10.1016/S0040-1951\(97\)00016-4](https://doi.org/10.1016/S0040-1951(97)00016-4).
- Poulet T, Veveakis M. A viscoplastic approach for pore collapse in saturated soft rocks using REDBACK: an open-source parallel simulator for rock mechanics with dissipative feedbacks. *Comput Geotech*. 2016;74:211–21. <https://doi.org/10.1016/j.compgeo.2015.12.015>.
- Poulet T, Paesold M, Veveakis M. Multi-physics modelling of fault mechanics using REDBACK: a parallel open-source simulator for tightly coupled problems. *Rock Mech Rock Eng*. 2016;74:211–21. <https://doi.org/10.1007/s00603-016-0927-y>.
- Ranjith PG, Viete DR, Chen BJ, Perera MSA. Transformation plasticity and the effect of temperature on the mechanical behaviour of Hawkesbury sandstone at atmospheric pressure. *Eng Geol*. 2012;151:120–7. <https://doi.org/10.1016/j.enggeo.2012.09.007>.
- Rudnicki JW. Shear and compaction band formation on an elliptical yield cap. *J Geophys Res*. 2004;109:355. <https://doi.org/10.1029/2003JB002633>.
- Rutqvist J, Wu Y-S, Tsang C-F, Bodvarsson G. A modeling approach for analysis of coupled multiphase fluid flow, heat transfer, and deformation in fractured porous rock. *Int J Rock Mech Min Sci*. 2002;39:429–42. [https://doi.org/10.1016/S1365-1609\(02\)00022-9](https://doi.org/10.1016/S1365-1609(02)00022-9).
- Rutter EH, Glover CT. The deformation of porous sandstones; are Byerlee friction and the critical state line equivalent? *J Struct Geol*. 2012;44:129–40. <https://doi.org/10.1016/j.jsg.2012.08.014>.
- Schmidt R, Seithel R, Stober I. Verbundvorhaben "StörTief" - Die Rolle von tiefreichenden Störungszonen bei der geothermischen Energienutzung - Teilprojekt C Südwestdeutschland. 2016.
- Schmidt RB, Bucher K, Drüppel K, Stober I. Experimental interaction of hydrothermal Na-Cl solution with fracture surfaces of geothermal reservoir sandstone of the Upper Rhine Graben. *Appl Geochem*. 2017;81:36–52. <https://doi.org/10.1016/j.apgeochem.2017.03.010>.
- Serdengecti S, Boozer GD. The effects of strain rate and temperature on the behavior of rocks subjected to triaxial compression. In: *Fourth symposium on rock mechanics*, Pennsylvania, 1961. p. 83–97.
- Settari A, Al-Ruwaili K, Sen V. Upscaling of geomechanics in heterogeneous compacting reservoirs. In: *SPE reservoir simulation symposium*. Society of Petroleum Engineers. 2013.
- Stober I, Bucher K. *Geothermie*. Springer geology. Heidelberg: Springer; 2012.
- Stober I, Bucher K. Hydraulic and hydrochemical properties of deep sedimentary reservoirs of the Upper Rhine Graben, Europe. *Geofluids*. 2014;15:464–82. <https://doi.org/10.1111/gfl.12122>.
- Terzaghi K. *Theoretical soil mechanics*. Hoboken: Wiley; 1943.
- Valley B, Evans KF. Stress state at the Soultz-Sous-Forrêts to 5 km depth from wellbore failure and hydraulic observations. In: *Thirty-second workshop on geothermal reservoir engineering*. Stanford University, Stanford, California, January 22–24. 2007.
- Vutukuri VS, Lama RD, Saluja SS. *Handbook on mechanical properties of rocks: testing techniques and results*, vol. 1, no. 1. 1st ed. Clausthal: Trans Tech Publications; 1974.
- Watanabe N, Blöcher G, Cacace M, Held S, Kohl T. *Geoenergy modeling III*. Cham: Springer International Publishing; 2017.
- Wong T-F, Baud P. The brittle–ductile transition in porous rock: a review. *J Struct Geol*. 2012;44:25–53. <https://doi.org/10.1016/j.jsg.2012.07.010>.
- Wong T-F, David C, Zhu W. The transition from brittle faulting to cataclastic flow in porous sandstones: mechanical deformation. *J Geophys Res Solid Earth*. 1997;102:3009–25. <https://doi.org/10.1029/96JB03281>.
- Zhang J, T-F Wong, Davis DM. Micromechanics of pressure-induced grain crushing in porous rocks. *J Geophys Res*. 1990;95:341. <https://doi.org/10.1029/JB095IB01p00341>.
- Ziegler PA, Dèzes P. Evolution of the lithosphere in the area of the Rhine Rift System. *Int J Earth Sci*. 2005;94:594–614. <https://doi.org/10.1007/s00531-005-0474-3>.
- Ziegler PA, Schumacher ME, Dèzes P, van Wees J-D, Cloetingh S. Post-Variscan evolution of the lithosphere in the Rhine Graben area: constraints from subsidence modelling. *Geol Soc Lond Spec Publ*. 2004;223:289–317. <https://doi.org/10.1144/GSL.SP2004.223.01.13>.
- Zimmerman RW. Coupling in poroelasticity and thermoelasticity. *Int J Rock Mech Min Sci*. 2000;37:79–87. [https://doi.org/10.1016/S1365-1609\(99\)00094-5](https://doi.org/10.1016/S1365-1609(99)00094-5).
- Zoback MD. *Reservoir geomechanics*, 5. print. Cambridge: Cambridge Univ. Press; 2011.